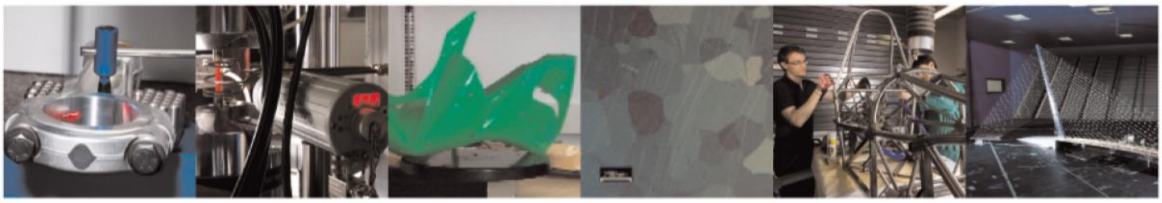

A new solution for assessing the printability of 17-4 PH gyroids produced via extrusion-based metal AM

Paolo Parenti, Dario Puccio, Bianca Maria Colosimo, Quirico Semeraro

This is a post-peer-review, pre-copyedit version of an article published in Journal of Manufacturing Processes. The final authenticated version is available online at: https://doi.org/10.1016/j.jmapro.2021.12.043

DIPARTIMENTO DI MECCANICA ■ POLITECNICO DI MILANO
via G. La Masa, 1 ■ 20156 Milano ■ EMAIL (PEC): pecmecc@cert.polimi.it
http://www.mecc.polimi.it
Rev. 0

A new solution for assessing the printability of 17-4 PH Gyroids produced via extrusion-based metal AM

Authors

Paolo Parenti[1], Dario Puccio[1], Bianca Maria Colosimo[1], Quirico Semeraro[1],

[1]Department of Mechanical Engineering, Politecnico di Milano, Via La Masa 1, 20156, Milan, Italy

Keywords

Additive Manufacturing; Gyroid; Lattice; Bound Metal Deposition; Extrusion-based AM; Regression

Abstract

Robust assessments of printability limits in complex geometries represents a key point for enabling the adoption and the spreading in industry of innovative Additive Manufacturing (AM) technologies.

The paper presents a novel solution to assess a printability map in metal AM able to capture the probability of producing a defect-free complex geometries embedding all the printing constraints and the geometrical specifications. The approach involves logistic regression as tool to assess the likelihood of obtaining defect-free complex geometries, depending on the process and the material at hands.

Besides proposing a new methodology which can be adopted for any printed geometry, the paper investigates the printing capability of a new emerging AM technologies based on extrusion of metal feedstock, such as the Bound Metal Deposition from Desktop Metal, for defect-free fabrication of an emerging lattice-based shape, known as Schoen gyroid.

The proposed method is based on combining quality data labeled by experts with failure mode analysis of the 3D printing process within a logistic regression model. The approach provides a final probabilistic map, in the design parameters space of the gyroids, where the likelihood of defectiveness is available at each location of the design space. The proposed methodology and the presented results support the development of robust defect- and waste-free part design approaches for AM.

Introduction and State of the Art

The design freedom allowed by Additive Manufacturing (AM) increased the interests in complex shapes components with enhanced properties [1]. Among these, nature-derived cellular materials inspire engineers thanks to their lightweight structure [2], their energy absorption capabilities [3], and their exceptional stiffness-to-weight ratio [4]. AM methodologies are enabling the production of these complex and geometrically controlled lattice structures, that are not easy to be manufactured via conventional methods. As mathematically defined geometries, lattice structures based on Triply Periodic Minimal Surface (TPMS) are receiving growing attention[5]. TPMS can be defined by an implicit function such as $f(x,y,z) = C$, where C dictates the offset of the surface. As definition of minimal surfaces, they have a mean curvature equal to zero in each point of the surface (i.e., the arithmetic mean of the principal curvatures is zero in each point, implying they are all saddle points), and they are composed by surfaces with no self-intersection which repeats themselves in three directions. These smooth infinite surfaces split a cubic cell into equal subspaces and are periodic in three independent directions. The control of these geometrical properties provides enhanced mechanical and physical behaviors with respect to other lattice types, that perfectly suits innovative engineering applications both in industrial [6] and biomedical [7,8] fields. Most of these attributes, above all the remarkable static resistance, come from their smooth surface with continuous curvature where no stress concentrations permeate throughout the structure, providing in addition good fatigue life [9,10]. Being the TPMS structures isotropic in nature, they are attractive candidates for usage as an infill structure in AM components [11]. Like strut-based lattices, TPMS structures found typical use in thermal applications because of the ability to create intricate geometries suited to the heat profile of the component to be cooled [12] due to their optimized fluid permeability, thermal conductivity [13,14] and heat exchange coefficients [15]. This complex geometry brings also the resemblance to wood and bone structures making TPMS good for suiting also tissue [16] and bone engineering [17,18].

Among dozens of TPMS structures, the Schoen-Gyroid is one of the most known one. As one of the most applicable TPMS, Schoen-Gyroid in sheet-network configuration can be approximated by the following trigonometric equation (Eq.1):

$$f(x,y,z) = sin(x)\, cos(y) + sin(y)\, cos(z) + sin(z)\, cos(x) = C \qquad \text{Eq.1}$$

When $C = 0$ there is no offset and the two subspaces defined by the surface are equal. A representation of a single unit cell of this surface (with $C= 0$) is shown in Fig. 1a, where $-\pi \leq x,y,z \leq \pi$. Volume can then be added to the gyroid thickness avoiding undesirable unparallel edges, Fig. 1b. This sheet-network type gyroid separates space into two oppositely congruent labyrinths of passages and without straight lines or planar symmetries.

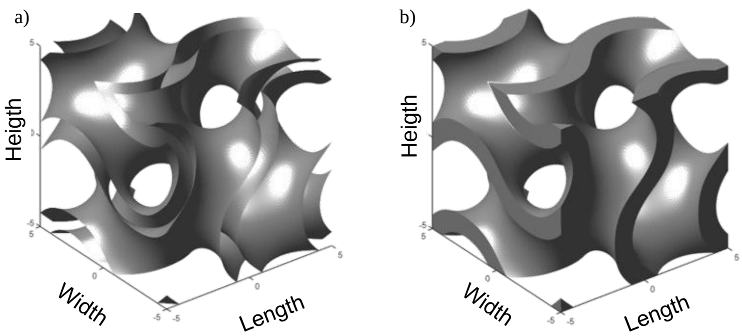

Fig. 1. (a) Zero thickness sheet gyroid, (b) with thickness (Relative Density RD=0.3),

The gyroids can be produced in both polymer, ceramic, and metallic materials. Metal gyroids structures are extremely performant thanks to the resistance and ductility of the material, and its thermal conductivity. Among metals, stainless steels, are one of the most interesting class of materials since they present, at relative low material cost, good corrosion resistance and good mechanical properties at high temperatures. This makes them ideal for thermal exchange and dissipation components.

Metal gyroids are typically manufactured in industry via Laser Powder Bed Fusion (L-PBF) [10], [15],[19] and Electron Beam Powder Bed Fusion (E-PBF) [8]. In the last years, industrial-ready binder-based AM technologies such as Extrusion-based processes (also called Feedstock Extrusion or metal Fused Filament Fabrication or Metal Fused Deposition Modeling) [20] and Binder Jetting [21] have been starting to come into role. With respect to power-beam AM, binder-based techniques can easily work with materials that suffer thermal stresses (as brittle ones) or that show poor absorption capacity of the irradiated beam power (as copper with laser beams). The production paradigm of these binder-based technologies is based on the decoupling between the shaping phase (printing) and densification phase (sintering). Thanks to that, parts do not require heat treatments to release thermal stresses or homogenize microstructures since no power beams are adopted and thermal cycles are conducted in a slower and controlled way. Since this production routine is not involving material's properties such as electrical conductivity (leading the E-PBF process) or laser absorption (leading the L-PBF process), it opens the possibility to produce both standard (such as 316L [22], Titanium alloys [23,24]) and difficult-to-AM materials (such as Tungsten alloys [25,26] , pure Copper [27,28], Silicone Steel [29]and Ceramics [30–32]).

In this binder-based AM scenario, metal Feedstock Extrusion is the most affordable technology from both the economical and the required user experience skills point of views. Despite the literature does not report specific studies on the manufacturability of gyroids through it, this process can be considered a cost-effective alternative for successful metal gyroids production. This is true especially when the size of the features required is not ultra-fine [33,34] and when the printing is not asked to produce extremely low wall thicknesses, being the extrusion process of an FFF type [35,36].

Bound Metal Deposition for gyroid 3d printing

The most currently known metal Feedstock Extrusion system on the market is the *Studio System* from Desktop Metal Company [37] that implements the Bound Metal Deposition (BMD) process. It is an integrated system (that also includes the debinding unit and the sintering furnace), and its peculiarity is the removable supports concept. This feature consists in the use of a ceramic interface material that helps releasing the part from the supports after sintering, without the use of any cutting operation as it is indeed required when the supports are made of build material (as in L-PBF and E-PBF parts) [38]. The BMD process is composed of three main phases: I) Printing, II) Debinding, III) Sintering. Except for how the green part is formed, BMD follows essentially the same steps as MIM but entailing the typical, greater, AM design freedom, albeit with a rougher surface finish and slightly increased porosity. The printing phase is essentially a Fused Deposition Modelling (FFF) like that of polymers [39], but a composite mixture of multi-component thermoplastic polymeric binder and build atomised material powder, i.e., feedstock, is used, Fig.2. The feedstock material is proprietary in BMD and is contained in cartridges in form of small rods that are extruded through a heated nozzle. The green parts are typically printed about 18% larger than the final parts to compensate for metal shrinkage (densification) occurring in the furnace sintering. After printing, the parts show a relatively soft nature becoming more brittle after the debinding step. The primary binder removal takes place in a warm chemical debinding bath using a liquid solvent, after which the brown part is removed, Fig. 2. The secondary binder components are removed during the pre-heating stage of furnace cycle i.e., thermal debinding after which the parts are sintered to allow for densification, where a final density of up to 95-98 % can be achieved [40], Fig. 2. Overall, this thermal process is carried out in a Hydrogen – Argon mix (H_2+3%Ar) gas mix and takes about 40 hours, depending on the size and material of the components.

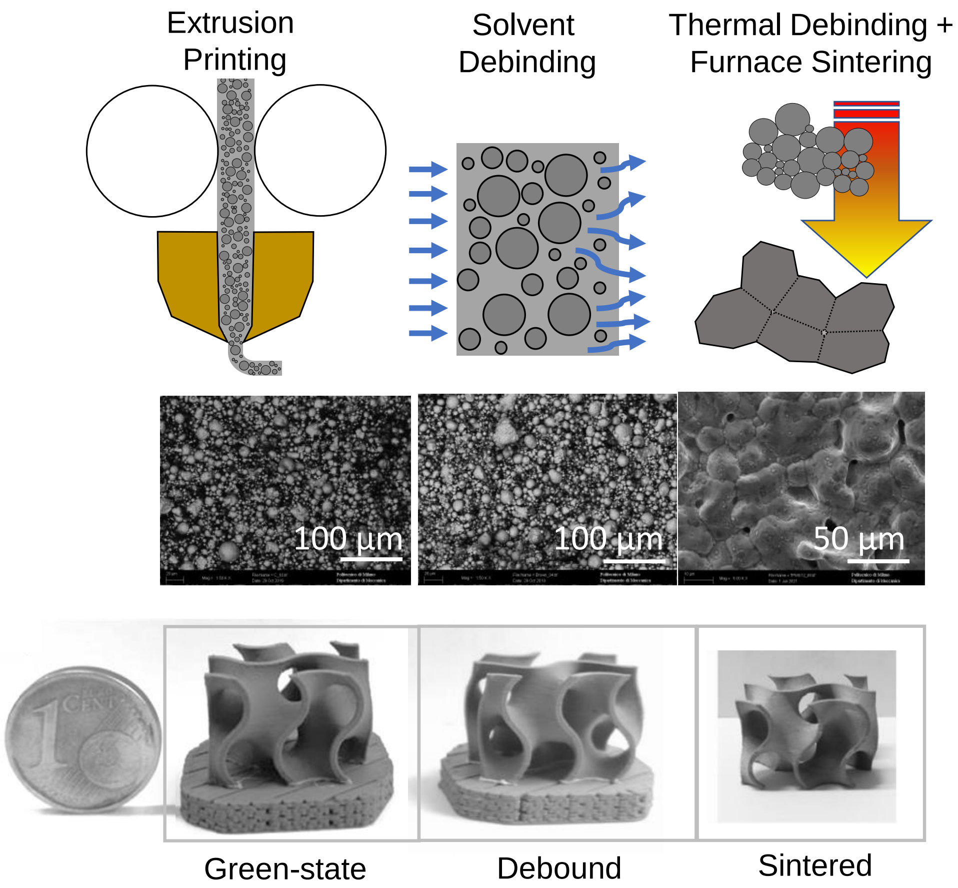

Fig. 2. Bound Metal Deposition process for 17-4 PH gyroid printing: green, brown and sintered parts along with feedstock material microstructure in the three different states in the three different states

Regardless of the 3D manufacturing methodology adopted, process constraints must be considered in the design workflow of lattice structures, considering the specific building materials involved and the nature of the different AM technologies adopted [41]. Therefore, the evaluation of the printing capability of these complex geometries for a specific geometry/process/material combination is a key enabling aspect.

With respect to complex geometry printing, BMD can show some limitations which can prevent the successful printing of the parts. The maximum achievable size not only depends on the building chamber size, but it is usually constrained by the maximum part size that can be effectively sintered without structure cracking or warping due to the shrinkage densification and gravity effects [34]. In terms of minimum printing size, it is not only the nozzle diameters that create a lower limit but in case of complex shapes as the gyroids, very intricate toolpaths can result in unsuccessful printings. For the same reasons, despite nominal achievable material density can reach high levels on standard geometries, complex toolpath can play big role by introducing material density lacking [25], therefore limiting the final material resistance.

For these reasons, providing the information regarding BMD process constraints in a synthetic and clear form is crucial for allowing design engineers to integrate BMD in their workflow. Ideally, the availability for each geometry/process/material combination of formalized knowledge, like printability maps identifying the geometrical parameters that can be achieved considering the specific process constraints, can trigger the capacity for design engineers to tune the specific application and fasten the design process and development. For instance, regarding gyroids, a deterministic map of manufacturable design spaces in terms of unit Cell Size and Relative Density is presented in [42] for SLS printing of polymer lattice structure is proposed. It pivots on the nominal minimum achievable thickness by the AM process. Experiments however showed that process deviations occurred to relatively big extent in terms of obtained Cell Size (2%), Relative Density (10%), and wall thickness (3%). This is an important aspect since small geometrical variations in the nominal characteristics can in fact lead to significant variations in terms of structural properties of the lattice structure

[43]. The achievable quality of commonly adopted AM processes in metal gyroid is quite high but characterized by some typical defects which strictly derive by the specific process technology adopted. Focusing on the defects related to the geometrical defects, powder sticking (or dross) is present in the overhang regions of the gyroids produced by L-PBF, due to the common adoption of support-free bed printing [6]. This problem is typically affecting the overall surface quality and can reflect into a direct specific impact on functional heat dissipation properties and it can also exacerbates the accuracy errors on wall thickness and Relative Density [44,45]. Similar defects, but with different root cause, can be generated in metal feedstock extrusion of TPMS gyroids, where the cause is not an excess of energy input into the powder bed, but the lack of a support structure where the feedstock can be deposited. In L-PBF these deviations from the designed Relative Density have been reported to be around 10-15% in absolute value [10],[46], while no data has been reported for metal-FFF. A consequence that can be extended to both the technologies is that the presence of these geometrical errors can affect the structure mechanical behaviour reducing also its predictability trough numerical modelling [6],[9],[47].

Other type of defects reported in [48,49] as geometrical deviation, presence of cracks, porosity and others, are originated from the laser beam and the process parameters and conditions which are different from what rules the metal FFF. Also the defect generated in polymers FFF have a different root cause, indeed mechanical behaviours seem mostly governed by the overall geometrical parameters design and by the boundary conditions, rather than manufacturing errors [36],[50]. However, when moving to metal-FFF, also the debinding and sintering phases effects can introduce uncertainties in the process.

All the above-mentioned studies confirm that studying the manufacturing process of gyroids is a worthwhile and key enabling step. However, tracing how the process outcome affects the final gyroid mechanical performance is not trivial since manufacturing errors, as well as the final mechanical performances, are geometry and machine dependent [45],[51]. Advanced data-driven techniques, such as machine learning, can help in this case, supporting the development of prediction models of metal gyroid final performances (e.g., deformation energy) starting from 3D printing process parameters [52]. Among these techniques, logistic regression is an effective statistical tool that can be helpful for characterization of manufacturing systems and processes [53]. Despite, to the authors' knowledge, logistic regression has never been applied to 3D printing methods, thanks to its characteristics and properties it can suit also the AM case [51].

The literature analysis confirms that, together with the raising interests in metal TPMS geometries, there is a conjunct need of robust process capability characterization of newly market available AM techniques such as the BMD.

The objective of this work is therefore developing a new methodology for obtaining the printability limits of gyroids when produced via BMD, implemented by the Desktop Metal Studio System+ [37].

The method must be capable to produce informative mapping (i.e., a printability map) of the process capability in the design range of gyroid parameters. It must be capable to deal with the wide range of defects that could affect the produced BMD gyroids and it must be robust with respect to process uncertainties in a way that the produced outcome is readily integrable into design-for-AM approaches.

The manuscript starts with the presentation of the gyroid geometry and the experimental approach. BMD process constraints in gyroid manufacturing are then introduced and put into relations with the spectrum of possible manufacturing defects. After this, the work presents and analyses the experimental printing results. Then, the proposed logistic regression model, as a data-driven tool for printability map definition, is presented and discussed.

Gyroid printing setup and BMD constraint

The parameters that determine the gyroid geometrical characteristics are three, as following:

- The Relative Density (RD) is defined as the ratio between the volume of the gyroid and the volume of the cubic unit cell containing the gyroid, $\bar{\rho} = V_{TPMS} / V_{unitcell}$.
- The unit Cell Size (L) is defined as the edge length of the cubic unit cell containing the gyroid.
- The wall thickness defined as the distance between two adjacent points lying on the profile of the gyroid walls obtained by sectioning with a plane along one of the principal directions.

Once two of the three parameters are imposed, the third one can be computed. Typically, the two independent parameters used by designers are the Relative Density and the unit Cell Size, while the thickness is derived consequently.

The most dominant limitation of the BMD with respect to gyroids regards the minimum printable wall thickness. To the authors' knowledge, no relation between the gyroid wall thickness and the Relative Density and unit Cell Size in sheet-network gyroids has been proposed in the literature. Therefore, it is derived through a numerical procedure. Since for certain levels of Relative Density, bigger than 50%, the wall thickness in sheet-gyroids becomes uneven along the surfaces [9], the investigations were limited to this parameter range, but can further extended in case of larger RD by simply considering the minimum values of the gyroid wall thickness. The gyroids are generated using *MSlattice* [54] with a mesh density per unit cell equal to 100. Once STL files of gyroids are obtained, *Blender* (v 2.92) is used for identifying and measuring the t_{wall} on the designed gyroids, given different combinations of L and RD (grid of 100 equally spaced points in the range of 5 < L < 50 mm and 5% < RD < 50%). A linear interpolation model is then found, Eq.2.

$$t_{wall} = 0.371 \cdot L^{0.997} \cdot RD^{1.051} \qquad \text{Eq. 2}$$

In the tested parameters range, fitting produces highly reliable results (R^2_{adj}=99.97%). Despite the exponents of L and RD are close to unit values, their positive effect on the fitting quality emerges for big values of L and RD and therefore they are maintained in the model. The wall thickness of the gyroids increases in a linear fashion with both L and RD thus producing an overall hyperbolic behaviour identifying iso-thickness curves, as shown in Fig.3.

Two iso-thickness curves constrain the processing window (i.e., the area were successful sintered gyroids can be obtained), given by the minimum feature suggested by the machine producer through the slicer SW (t=0.6 mm) and the maximum wall thickness to have appropriate debinding after printing (t=10 mm). The minimum achievable thickness of the sintered gyroid walls is linked to the process resolution, i.e., the size of the minimum achievable feature. This not only determined by the printer nozzle diameter, i.e., 0.25 mm, but also by the toolpath strategy given by the slicer SW and by the amount of shrinkage occurring in sintering. In the case of BMD, a generic threshold at 0.6 mm is suggested by the machine producer on the final part thickness, Fig.3. It must be pointed out that this value is indicative for any kind of printed geometries and therefore it might be not accurate when complex geometries like gyroids are printed. The system manufacturer implemented this limit as a rule in the slicing software which constraints a printed feature at green state to be formed at least by two adjacent feedstock strands (the features that would require less than 2 strands are printed with 2 strands, anyhow). Therefore, rather than a suggested minimum thickness limit, this becomes an imposed SW constraint that acts during the green state printing process. Eventually, this limit turns into a sintered wall thickness limit basing on the sintering shrinkage and on the relative oversize compensation that the SW adopts.

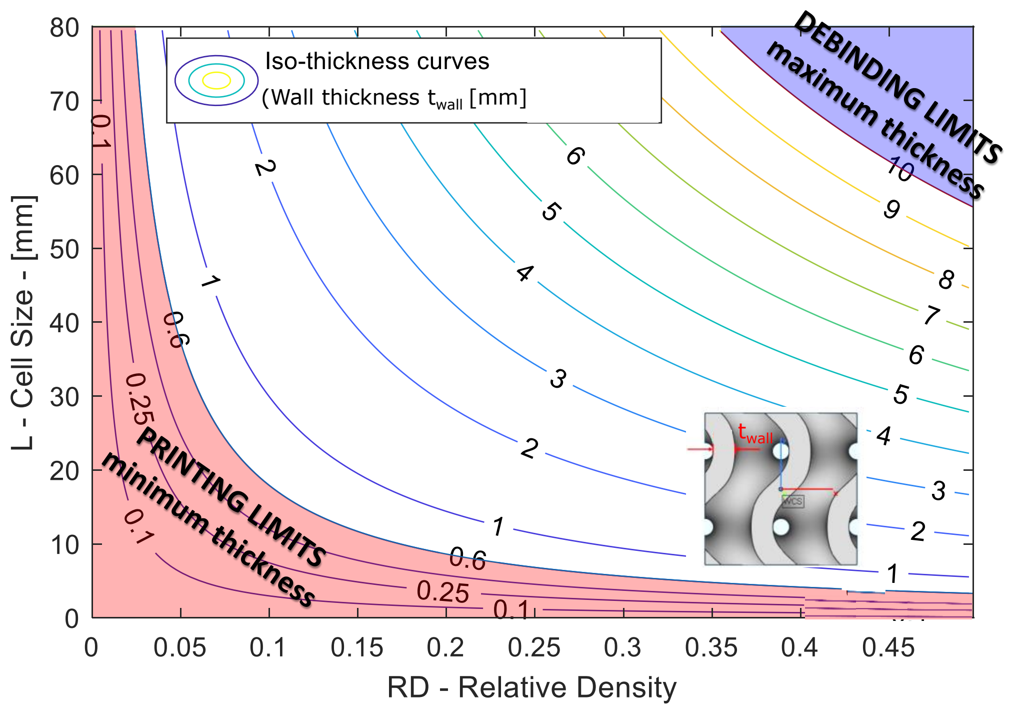

Fig. 3. Minimum wall thickness curves (t_{wall} in Eq.2) of the sheet gyroids and nominal printability limits of gyroid BMD printing

The second unfeasibility region constraining the maximum wall thickness is due to the maximum debindable wall thickness, as depicted in Fig.3. Debinding is critical since an inadequate debinding phase can lead to defects during sintering, such as cracking, blistering and the appearance of internal voids. A prescribed limit of 10 mm exists in BMD on wall thickness for fully dense walls and can be overcame only if a partial material infill is adopted, as suggested by the system manufacturer. In this case, the software does not impede to launch

debinding of bulky parts, but the imposed debinding cycle time exceeds reasonable values. A part from that, the open structure and the smooth surface of the gyroid geometry assist the solvent flow giving optimized debinding results [55].
Given the complex geometry of the gyroids, their printability strongly depends on the selected printing setup. On one side, given the total symmetry of the considered single-cell Schoen-Gyroid, and supposing a good printer accuracy on the printing plane, the selection of the printing orientation is not critical. In fact, all the combinations of one gyroid face lying down, give the same toolpath in X, Y and Z, directions. As in the FFF process, BMD requires supports in the overhang regions. Gyroids show several regions where the subtended angle (between the local normal and the printing direction) exceeds the maximum values of 55° which is the nominal limit of the slicer for support-free printing. The use of external supports (from the raft to the part) as well as of internal supports (between the gyroids walls), is suggested by the slicer, Fig.4. In general, the presence of supports represents a significant problem for finishing, as they can be hardly removed especially, when multicellular structures are considered, despite the presence of ceramic interface layer. Furthermore, the presence of supports could also create local stress intensification in sintering due to the presence of ceramic interlayer. In order to manufacture an unsupported and free-standing (without walls bounding the cell) single cell gyroid, a feasible printing configuration must be identified to avoid printing problems related to unsupported overhanging parts, Fig.4. One solution consists of printing a larger cell in one direction. An example is given in Fig. 5, where the structure with a ¼ extra cell in both sides in x direction does not show critical overhanging regions that would require support structure. With this modification, open, free-standing gyroid structures can be printed using extrusion-based processes, but still defects may rise.

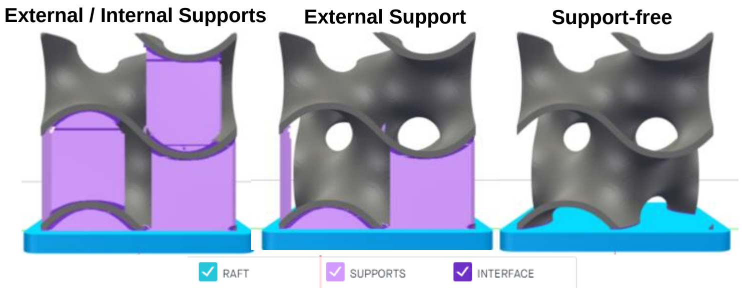

Fig. 4. Single cell gyroid printing setup with different support strategy

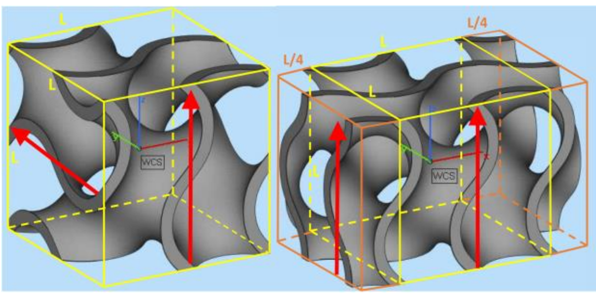

Fig. 5. Single cell (1L x 1L x 1L) gyroid configuration versus the extended (1.5L x 1L x 1L) single cell configuration that is selected for BMD printing

Modelling quality in gyroids

Atlas of possible defects

Different types of defects are observed to originate in all the three distinct phases of the BMD process, Fig.6. They can be categorized as reported in Table 1, putting in evidence the way the typical defects of the feedstock extrusion processes are exacerbated by the characteristics of the printed TPMS gyroid geometry.

- Green-state defects

The printing-related defects found at green-state can be grouped mainly into three categories: nozzle clogging, deposition strategy and part design. Some of them are shared with standard polymer FFF process implementations, some are not. Material agglomerates deposited on the part surface are related to a partial or temporary clogging of the nozzle, as well as the “stringing”, a common defect and well known in the FFF process, which consists of strings of extruded material, smaller than the extruded beads, deposited on the printed layer or on another surface of the component. This usually happens when the material keeps flowing

out from the nozzle while the extruder is moving out from the deposited object. The stringing of the build media represents a minor failure, since it can be processed and removed while part is still in "green" state. Instead, the stringing of the interface media can cause intra-layers inclusions which can develop in cracks or local porosities after sintering.
A defect related to the deposition strategy is the formation of "air gaps" between adjacent depositions, which is observed in the manufacturing of the gyroids, especially when the part sections are thicker. These gaps are relevant and cannot be compensated by the densification in sintering, therefore they survive leaving a defect inside the material and reducing the overall density. Other defects reported, that can be addressed to the design choices, are the presence of geometrical distortion in the overhang regions, and the partial collapse. The latter occurs when the printed feature presents a small footprint connected to the build plate, making the part not able to sustain the forces applied from the printhead in the layer deposition process. The consequence of this type of defect can be the partial or total collapse of the structure in the sintering process.

- Brown state defects

The geometry of gyroid fosters the solvent and thermal debindability of the components since the open channels allow the fluids and/or the gas to flow out easily from the internal walls [55]. The fact that all the gyroids, the finest and taller ones included, survived the solvent debinding step means that the structural resistance of the brown material and the self-supportness of the gyroid geometry compose a good matching for the BMD process. The most prominent defect observed after debinding at brown-state is the structure deformation/warpage. The printing residual stresses are released in this phase since debinding decreases (by washing out a component of the binder), the binder structural resistance. Massive TPMS parts with big Relative Density, with thick walls were observed to be mostly subjected to warping phenomena.

- Sintered state defects

The last phase of BMD process can propagate defects originated in the previous phases or generating new ones. Cracks and delamination can develop due to the sintering stresses (shrinkage occurring during sintering might be not uniform). The above-mentioned air gaps in sintering are a consequence of the air gaps generated in the printing phase. Crack-free parts are obtained for all the gyroid printed without internal and external support. However, alternative testing conducted on single-cell supported externally (Fig. 4) produced gyroids affected by severe cracking in the region close to the supports.

Table 1. Defects observed in the BMD of TPMS Gyroids

Occurrence	Defect Type	Causes
Printing / Green-state	Stringing / Agglomerate of Build Media	Partially clogged nozzle; deposition and retraction strategies
	Stringing/Inclusions of Interface Media	
	Printed-Air Gaps (Air-voids)	Deposition strategy / nozzle size
	Overhangs defects	Deposition strategy / thin wall design
	Partial Collapse	
	Geometrical Inaccuracies	Part design / nozzle size
Debinding / Brown-state	Warpage	Part design / printing residual stresses
Sintering / Sintered state	Cracking / Delamination / Collapse	Sintering thermal stress – Shrinkage / gravity
	Warpage /Geometrical Deviations	
	Porosity	Printed-air gaps
	Inaccurate Final Dimensions	Shrinkage/incorrect oversizing

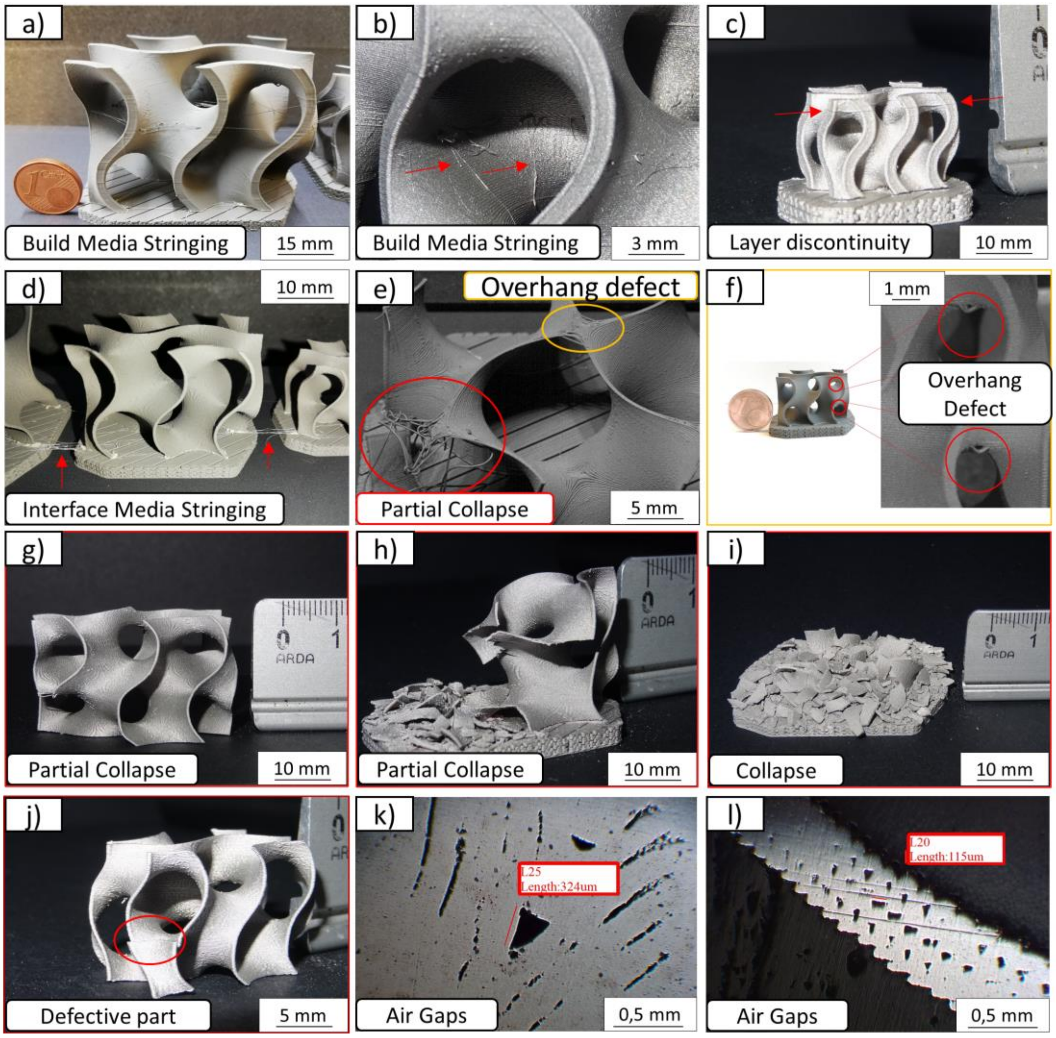

Fig. 6 Observed defects on gyroids: (a) Build media stringing at green state and (b) detail on sintered state; c) Layer discontinuity (sintered) d) Interface media stringing (green); e) Onset of partial collapses and defects in overhang region; f) Overhang defects (green); g/h/i) Structure collapse (sintered); j) Structure with detached zone (sintered); k/l) Air gaps (sintered)

Definition of quality acceptance criterium

For assessing the printability of gyroids a quality indicator is needed. This quality assessment procedure is here based on both qualitative and quantitative criteria. The qualitative criterion consists of a visual evaluation based on the atlas of defects and conducted after the sintering of the produced gyroids. A panel of three experts independently evaluates the printed gyroids, considering either the presence of consistent damages or of less severe defects. The multiple qualitative evaluations given by the experts are combined with the quantitative criterion that, is the deviation from the nominal Relative Density, being this latter a relevant design parameter for such geometries.

For the purpose of the study, a threshold of 5% of absolute RD error (i.e., *"errRD"* deviation of actual RD from the nominal designed one) is fixed (Table 2), basing on typical errors in metal gyroid production ([10],[46]).

For the tested BMD gyroids, little variations around the selected threshold does not introduce big variation in the printability map and therefore a detailed sensitivity is not herewith discussed.

The RD_{real} is estimated, Eq.3, starting from the measured sample weight (m), measured material density (ρ) and the measured bounding box ($L_x \cdot L_y \cdot L_z$):

$$RD_{real,i} = \left(\frac{m \cdot \rho}{L_x \cdot L_y \cdot L_z}\right)_i \qquad \text{Eq.3}$$

Finally, the judgements from both criteria are combined, when both criteria give the value 0 the part is classified as acceptable part, else as failed. Being a binary logistic regression model, only two levels are defined. Enhanced logistic regression fitting with ordinary logistic regression models can be adopted when the classification of the printings requires more differentiated levels [56]. The acceptance criteria defined for the adopted binary logistic regression analysis are summarized in Table 2.

Table 2. Parts quality acceptance criterium used in the analysis

Quality	Visual assessment		Error on Relative Density (*errRD*)
Level 0	acceptable parts, with no (or negligible) external surface defects	AND	-5 % < *errRd* < +5%
Level 1	collapse (partial / complete), warping, surface defects	*OR*	*errRD* ≥ +5 % or *errRD* ≤ -5 %

Experimental testing

Materials

The selected material for conducting the experimental testing is 17-4 PH, a martensitic precipitation hardening stainless steel with outstanding combination of high strength, corrosion resistance and good mechanical properties as toughness and yield stress. The declared achievable sintered density from the machine producer is 7.6 kg/dm^3 [34]. The proprietary slicer *Fabricate* is used for processing the generated STL files of the gyroids.

Design of experiments

Since the scope of the work is proposing a method to evaluate the printability of gyroids in their geometrical design space, several tests are conducted by varying L and RD. For the selection of L and RD values, particular importance is given to investigate the low gyroid's wall thickness range, being this limit more critical than the upper limits caused by the debinding cycle [37]. Regardless of the tested ranges of this study for L and RD, they were chosen between 10 and 30 mm and between 4% and 36.8 %, respectively. The reasoning behind the choice of this design area is because, as per the above analysed literature, most of the gyroids' applications fall in these ranges. Experimental replicas are carried out to test BMD repeatability. Large presence of process uncertainties is expected in the critical region around nominal minimum thickness limit of the machine. (i.e., around 0.6 mm of wall thickness). Therefore, rather than running an equally spaced factorial plan, logarithmic spanning of the tested points (see Appendix A, Table A1) is designed to densify the investigation on gyroids with small thickness, as can be seen in Fig.3. For the same experimental effort, this point distributions improves the quality characterization capacity in this critical zone.
In total 16 different gyroids geometrical conditions are tested, three replicas for each condition, for a total of 48 printed specimens. Four different gyroids are deposited in each printing cycle, all with different L and RD. The debinding and sintering phase are carried out 16 parts at a time, i.e., one replica at a time.

BMD process parameters

Since a baseline printability analysis is here evaluated in terms of gyroids geometrical parameters, the nominal BMD process parameters and standard printing setup suggested by machine producer are adopted.
The finest extrusion nozzle with diameter 0.25 mm is used along with the proprietary *UltraFine+* printing strategy. Extrusion temperatures are set to 165°C and 65°C for the nozzle and the bed, respectively. Line width and Layer Height are set to 0.3 and 0.1 mm, respectively. Except for the presence of supports, the printing setup and parameters are selected following the manufacturer SW guidelines. The adopted base i.e., the raft (Fig.4) is composed of 18 layers separated by 3 layers of a conformal ceramic interface. A fully-dense line infill strategy along with conformal shell strategy of 0.9 mm is used for depositing the gyroids surface, Fig.7.
Gyroids are printed unsupported by avoiding the presence of any internal and external supports structures, as indeed suggested by the slicer. This study is carried out with nominal BMD process parameters (printing, debinding and sintering), as suggested by the proprietary *Fabricate* software. This gives a clear and direct picture of the BMD capability with this complex printing geometry when standard (and therefore disclosed) configuration is adopted. Figure 7 shows the long and quasi-continuous extrusion path in the horizontal plane during the modified gyroid printing. The periodicity of the gyroid along the vertical direction generates similar paths at different layers.

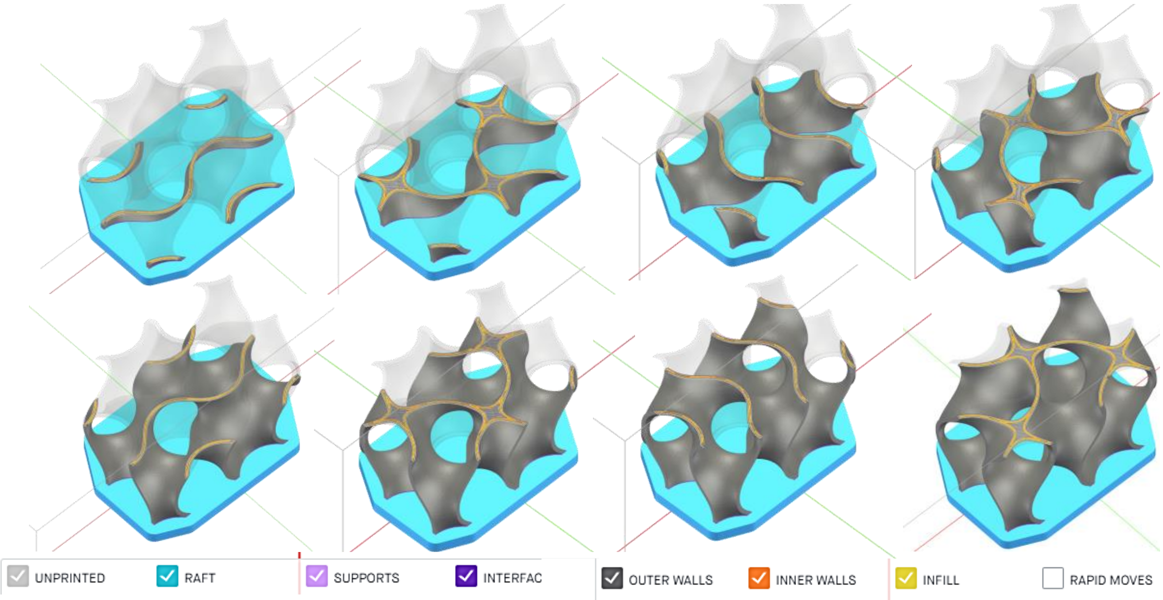

Fig. 7. Extrusion Toolpath of modified gyroid unit cell (L=30 mm, RD=0.061)

Inspection and measurement of the gyroids

The experiments are analysed in terms of both quantitative outputs i.e., the actual size and Relative Density of the gyroids, as well as their sintered material density and a qualitative assessment of their quality at sintered state. Optical Profilometer (Mitutoyo Quick Vision - 202) and manual calliper are used for size measurements (i.e., L). Mean density on the sintered gyroid material is measured via Archimedes' method through an electronic balance equipped with a Sartorius YDK 01 kit. The density (ρ) is derived as $\rho=Wa*(\rho fl- \rho a)/(Wa-Wfl)+\rho a$, where *Wa* is the air weight of the specimen, *Wfl* is the water weight of the specimen, ρfl is the density of deionised water at the measuring temperature of 20.3° (0.99814 g/cm^3) and ρa is the density of the air (0.0012 g/cm^3).

The Relative Density (RD_{real}) measure on the sintered gyroids is obtained by dividing the measured gyroids volume (i.e., specimen air weight divided by the actual material density) by the containing cube volume (i.e., obtained from the measured Cell Size). Scanning Electron Microscope (Zeiss EVO 50 XVP) is used for surface evaluation and microstructure analysis.

Printability evaluation through logistic regression

The new approach, here proposed for deriving a printability map of TPMS gyroids, is based on the execution of experimental printing tests of gyroids and on the application of logistic regression for modelling the printing quality outcome. Logistic regression is a common statistical technique which makes part of the category of the generalized linear models [57]. The logistic regression allows to derive the probability of an event (e.g., the printing failure) as a function of multiple predictors (e.g., the design variable of the gyroids, as the Relative Density and the Cell Size). This enables to evaluate the statistical boundaries separating the areas of the printability map (in the design space of gyroids) with successful and failed printings, associating in each of these conditions a probability. The probability ranges from one to zero. It has unit value when all the printing replica of a certain gyroid parameters condition result in good parts that match with the requirements. Its value becomes zero when a certain parameters condition is for sure producing failed specimens. It assumes values between one and zero, when only some replicas of the printed specimens match the requirements. This method therefore helps to characterize manufacturing systems that produce a process response that is not fully deterministic, as typically happens when working nearby the system limits. This effective statistical method can therefore produce the evaluation of robust printability limits, i.e., the gyroid parameters that can be surely printed successfully, without defects, and at the same time informing about the uncertain zone (the transitional zones of the success/failure probability) where the printed gyroids cannot fully match the quality requirements. this way, the product designer (integrating the gyroid geometry into a functional component) can integrate in the part design the actual constraints of the manufacturing process, being conscious about how close to the actual printing system limits the solution is. For instance, given two or more different combinations of Relative Density and Cell Size, that match the design requirement and the final gyroid functionality, the logistic regression printability map could help designers to choose the geometrical design parameters that are safer to 3D print or compare the different solutions in terms of the produced scrap costs.

The definition of the printability map through logistic regression relies on the evaluation of the quality of the manufactured samples. One pro of this technique is that can integrate both qualitative and quantitative quality indicators, therefore expanding the applicability on complex 3D printed components which are not easily measurable. Through the logistic regression, a quantitative measure of the uncertainty and scatter of the process quality response can be produced, supporting the identification of the actual process capability limits.
The parts are allocated to the class “acceptable” or “failed” basing on the qualitative and quantitative criteria above mentioned. The parts are judged “acceptable” only when both criteria are passed whilst in all the other cases they are judged as “failed”. Considering only two levels (0 for good parts and 1 for failed parts), the response y can be modelled through the ‘*logit’* link function [57] as a (Bernoulli) random variable which assumes the value 0 with probability π_0 for good samples, while it assumes unit value with probability $\pi_1 = 1 - \pi_0$ when a failed sample is observed, [53].
In the case of multiple number ($k > 1$) of predictors ($\boldsymbol{X}=x(k)$) , multiple logistic regression must be considered [57]. This regression model assumes that the natural log of the odds ratio (π_0/π_1) and the predictors **X** have a linear relationship, as Eq.4.

$$\hat{\boldsymbol{y}} = logit[\pi_0(\boldsymbol{X})] = ln\left(\frac{\pi_0(\boldsymbol{X})}{1-\pi_0(\boldsymbol{X})}\right) = \mathbf{X}\hat{\boldsymbol{\beta}} \qquad \text{Eq.4}$$

Where **X** is the matrix of the predictors (based on the factors L, RD and their interaction L · RD) and the vector of the coefficients $\hat{\boldsymbol{\beta}} = (\beta_0, \beta_1, .., \beta_k)$ is fitted by the maximum likelihood method , as one of the most efficient method [56]. The basic idea behind the maximum likelihood method is finding the coefficients values under which you would be most likely to get the observed results. In this work, the logistic regression model is fitted using the software Minitab 2020 (19.2020.1), considering the link function logit and the interactions through order 2.

Results and Discussion

Printing outcomes overview

With the prescribed process assumptions i.e., the use of default process parameters and of the self-supported single cell configuration, the experts judged the quality of the obtained samples in general acceptable while presenting several defects or even process failures in some conditions. Printing time is in line with the SW estimation, which spans from 2 hours (for the smaller gyroid) to 13 hours for the biggest part. Production time resulted fully deterministic with no sensible change among the replica at certain specific conditions. In the tested design space, 26 printings were successful whilst 22 printings out of 48 were not passing the quantitative and qualitative quality objective functions (i.e., parts obtaining the Quality Level 0, as indicated in Table 2). In 5 gyroid geometrical conditions (Run #6, #7, #8, #9, #11), the system produced uncertain response: one or two replica/s out of three failed while the remaining one/s passed (see Table A1 in Appendix A and Circled-Asterisk points in Fig.10). The successful printings are in line with the expectations which means they produced fully sintered gyroid cells that can be detached from the base by a simple manual operation and that are free from visible defects such as surface irregularities, warping, cracks, Fig.8. The shrinkage phenomenon occurring during the sintering phase is visible in Fig. 2, where the sintered part shows a dimensional reduction compared to green and brown state.
No noticeable quality difference is present among the successful sintered gyroids despite the different surface appearance and staircase effects, Fig.8. On the other, most of the printing failures, (15 samples) showed a partial collapse affecting the same small portion of the gyroids, in printing (the detailed description of these conditions and the occurred defects follows in the next paragraphs). A part of these samples (8 samples), affected by partial collapse, experienced a total collapse in the furnace treatment. Few ceramic particles contamination, that cannot be cleaned with blow air, is noticed on the gyroid walls in contact with the ceramic interlayer and the base Fig.8. No parts died in the solvent debinding cycle and mass reduction due to dissolution of the primary binder components were even among the samples (4.1% in mass). Out of the 16 different combinations of L and RD, 6 conditions showed a total printability i.e., successful sintered gyroids for all the three replicas tested. There are 5 conditions in which uncertain printing results are obtained, which means only one or two samples out of the three replicas is/are printed and sintered successfully. And in 5 conditions the parts are classified as failed, being affected by severe defect or a high variability in the response RD_{real}.

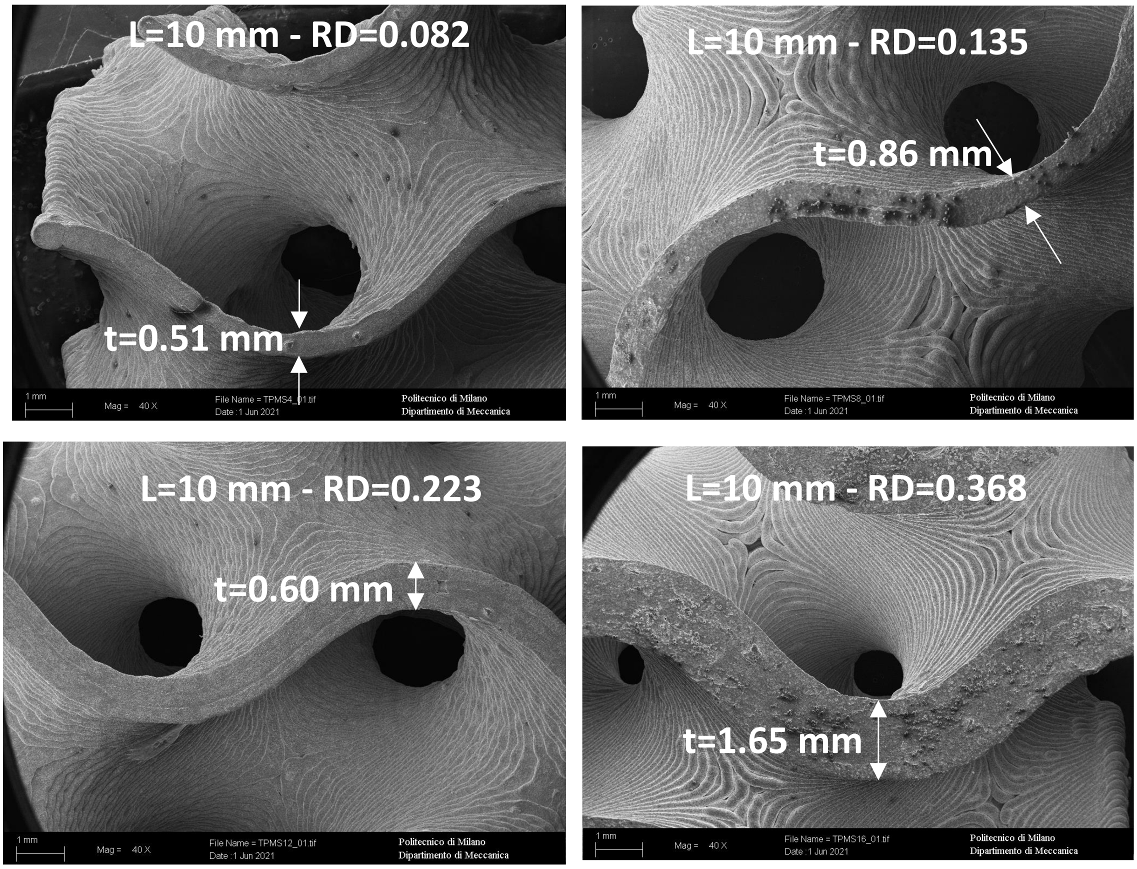

Fig. 8. Scanning Electron Microscope analysis of sintered gyroids. Indicated thickness *t* values are measured values.

Printing accuracy

Dimensional accuracy of the sintered gyroids, i.e., the amount of deviation of L_{real}, RD_{real} with respect to designed values, is acceptable for most of the conditions. Average percentage errors on L_{real} are about 1% in all the three directions, with limited variation among the replicas (Fig. A1b in Appendix A). Regarding the process repeatability on Cell Size L, the average standard deviation of the error for all the tests equals 0.08 mm, reaching a minimum value of 0.02 mm for the three replicas of Run #14 (nominal L=23 mm). The dimensional error on L increases for the smaller scale cells reaching 4% (i.e., 0.4±0.05 mm for the cells with L=10 mm, Run#4). The weight measures (air and Archimedes method) conducted on the sintered specimens revealed an average density of the parts around 7.39±0.067 g/cm^3 a slightly lower value (-2.7%) than the declared one for 17-4PH steel (7.60 g/cm^3), (Fig. A1a in Appendix A). However, some variations are observed for the specimens with smaller wall thickness that reach values smaller than 7.25 g/cm^3 (-4.6%). In any case, it can be noticed that the effect of the geometrical factors of the gyroids played a bigger role than the one played by the process with its pure variability. In fact, the material density varied within the replicas in a more limited way with respect to the variability of the material density between the different gyroid conditions. The errors committed by the system on the material density of the parts, together with the errors on the L determine the amount of deviation that the specimens showed on the Relative Density. The percentage error on this latter quantity (i.e., the percentage error between the RD_{real} and the nominal RD) resulted equal to 1.1±8.8 %. These errors are distributed quite evenly in the range ±4% but for specimens with smaller thickness they reach up to 40% of positive offset (gyroids have bigger actual RD than expected), Fig.9.

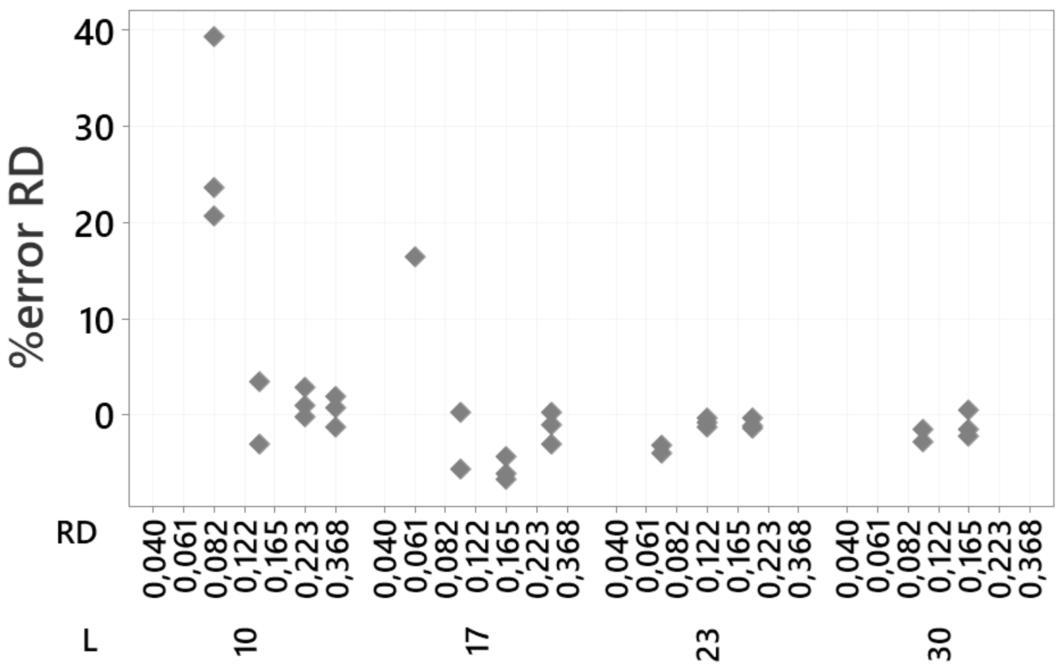

Fig. 9. Percentage Errors on gyroid Relative Density (%error RD= RD_{real} - RD / RD *100). Collapsed parts are not analysed, therefore the related points are missing in the graphs.

Feasible printing and failures

The analysis of the printings in the design space of gyroids confirms that successful manufacturing operations are obtained for all denser conditions at the relative various cell-size L values, Fig.10. Conversely, unsuccessful printings are produced for the least dense conditions for each relative L values. While most of the failures belongs to gyroids printed with biggest size i.e., L=30 mm, alternated successful outcomes are produced in the intermediate range of parameters (L=17 mm and 23 mm). Partial and total part collapse result to be limited in the top-left region of the design space while for the bottom areas, fracture-free sintered parts are obtained.

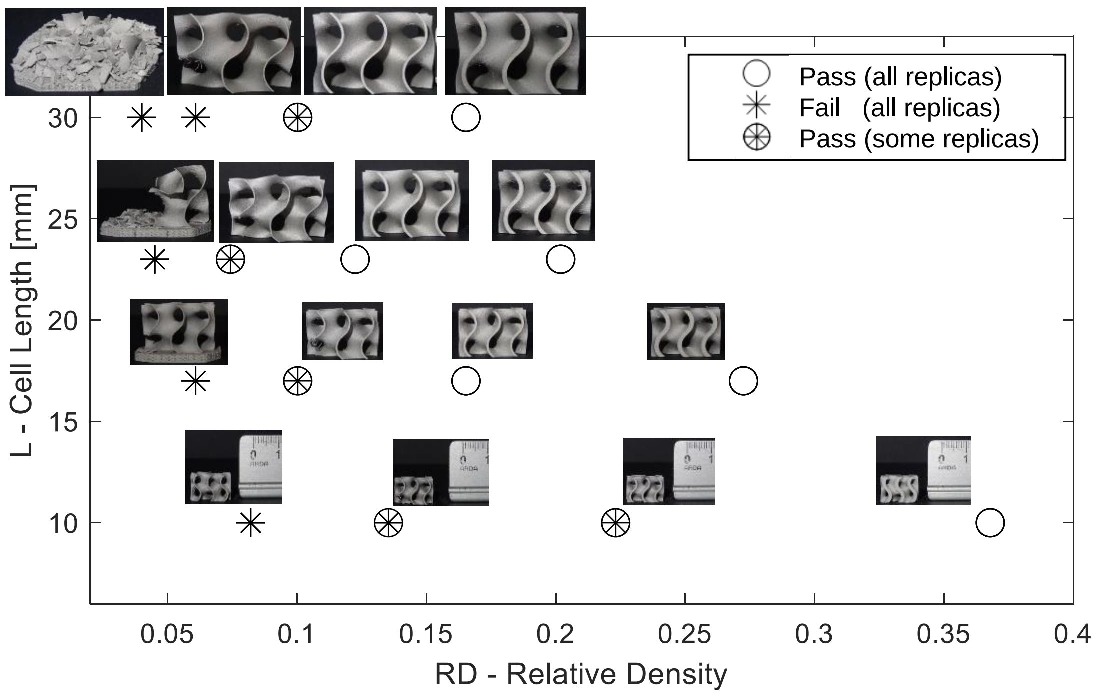

Fig. 10. BMD output performance during gyroid printing in the tested designed conditions

Being the BMD process chain long and being the support-free gyroids characterized by complex geometry and overhangs, a wide spectrum of defects emerged from the analysis. The occurred defects are mapped in Fig.11 in the design space of gyroids.

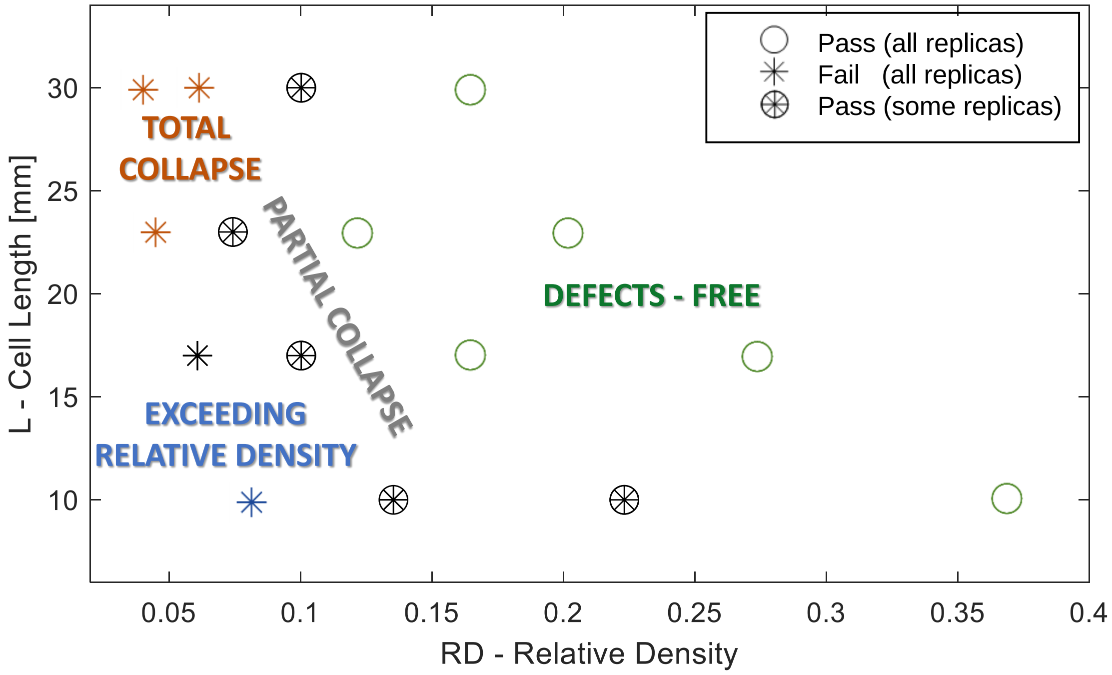

Fig. 11 Mapping of BMD printing defects in the gyroid design space

Extremely thin-walled gyroids with the smallest size did not show any collapse during printing and they are classified as “failed” because excess of material was deposited. Their nominal thickness is 0.358 mm, but their walls are printed using two strands of material causing their actual thickness to be around 0.52 mm and causing an excess of more than 5% with respect to the nominal Relative Density (first acceptance criterium). However, for them also the visual assessment judgment is not passed (second acceptance criterium) since their appearance is extremely irregular and characterized by surface irregularities. This suggests the fact that the machine, when asked to produce gyroids with wall thickness smaller than two beads (i.e., 0.6 mm), imposes the two beads toolpath but doing that it decreases overall printing quality.

Identified logistic regression model

The information gathered through qualitative and quantitative inspection, and conveyed into the Fig. 10 and Fig. 11, represents the input for the logistic regression model which is used to assess the 3D printability of the BMD metal gyroids. The identification of the binary logistic regression model is performed, and the fitted model equation is found, Eq.5:

$$y = -4.81 - 0.047\,L + 14.8\,RD + 1.98\,L \cdot RD \qquad \text{Eq.5}$$

The response y indicates whether a sample has been classified as acceptable or failed part, for each combination of the predictors L and RD, and π_0 is the associated probability of having an acceptable part. The coefficient table of the logistic regression model is reported in Table 3 (for a 95% of statistical confidence). The interaction term L·RD has a p-value of 0.055 and therefore is considered a significant term. Despite their p-value is above threshold, the individual terms L and RD are kept into the model to respect the hierarchy.
The model obtained is a probability function of the predictors L and RD. For a clear visual representation, the response map is obtained by projecting the probability surface onto the L-RD plane as shown in Fig.12. The iso-probability lines discriminate between the printable design space, with a success probability $\pi_0 > 0.9$, and the other regions characterized by a decreasing probability of good manufacturing the parts while moving towards the unprintable design space. Moreover, the interaction L·RD finds a graphical interpretation. For the highest value of Cell Size, L=30 mm, the 20/90% iso-probability lines lie within a range of RD 0.05 wide, indicating a sharp transition between failed and good parts. For instance, parts of L=30 mm and RD about 0.12 have strong probability of success while parts of Relative Density 0.07 are most likely going to fail. A different behavior is observed at lower size. At L = 10 mm the width of the 20/90% uncertainty span for RD increases up to 0.11 describing a wider process uncertainty region for small Cell Size values.

Table 3. Coefficient table for binary logistic regression

Term	Coef	SE Coef	95% CI	Z-Value	P-Value	VIF
Constant	-4.81	2.32	(-9.35; -0.27)	-2.08	0.038	
L	-0.047	0.110	(-0.263; 0.169)	-0.42	0.671	8.56
RD	14.8	18.1	(-20.6; 50.1)	0.82	0.414	7.37
L*RD	1.98	1.03	(-0.05; 4.00)	1.92	0.055	6.87

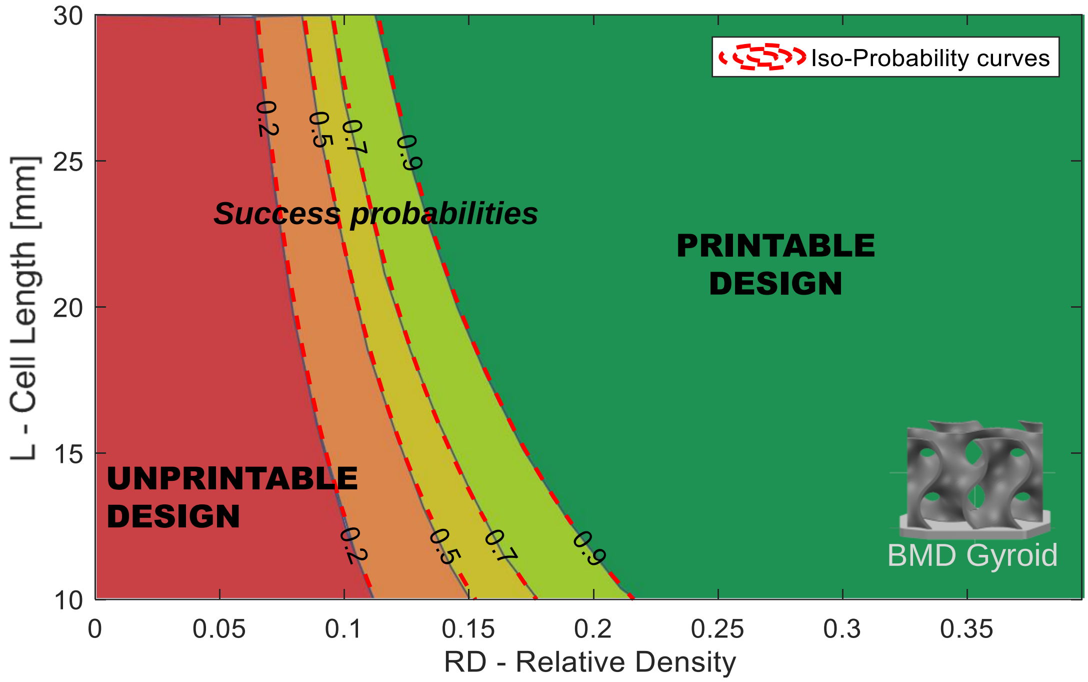

Fig. 12. Fitted logistic regression model plotted in the design space of BMD gyroids. Odds curves (Iso-Probability) in dotted red.

Printability limits evaluation

Printability map obtained by the application of logistic regression model resembles the map derived from the minimum printable wall thickness, Fig.13. Odds curves follow the same hyperbolic behaviour of the iso-thickness, but a degree of disagreement is found between the boundary limits of the two graphical tools. The nominal limits of 0.6 mm in wall thickness (that origins from the slicer software which forms a wall toolpath with a minimum number of two printing beads) falls in the area where the actual probability of success is rather low (between the 20% and 50%). So, BMD printing of gyroids with 0.6 mm wall thickness is not fully guaranteed, meaning that, interestingly the physical limitations of gyroid BMD exceed the constraints given by the Desktop Metal proprietary software. This is a clear example of the ability of this new methodology involving logistic regression. Not only support the product designers in finding the reliable BMD gyroid design region but can help the BMD process engineers in identifying the areas where the process struggles and deviate from expected performance, that eventually can require optimization. Such a probabilistic printability map can in fact drive technologists to carry out process optimization, for instance in terms of printing parameters tuning, by focusing on specific regions (as the identified transition regions between printable and unprintable gyroid design) saving resources with respect to a blind approach investigating all the geometrical design map.

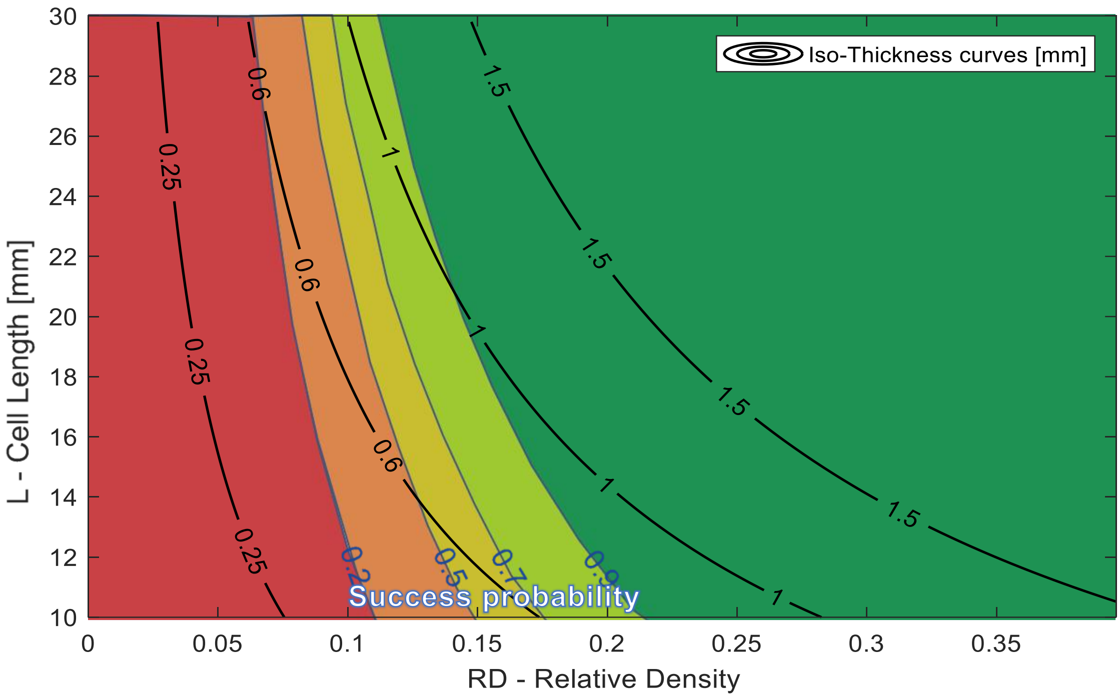

Fig. 13. Odds curves of successful printing along with iso-thickness of gyroids

Another strong point here is that, once collected the experimental quality data on printed parts, the map can be easily recomputed by modifying the quality function that divides the acceptable and fail regions. In this way, one can quantify the impact that quality requirements have on the overall printability of that geometry. At the same time, the evaluation of the printability of different lattice geometries is also easy since the method can be fed with any additional experimental data point.

This probabilistic approach could also serve at the production costs estimation / optimization, since the success and failure rates inform about scrap costs, both in terms of material and/or time resources. This latter point can also be used to compare different lattice geometries but also different AM technologies.

Finally, the shape of the odds curves can finally support the comprehension of the mechanisms involved in the defect generation, as discussed in the following paragraph.

Geometrical complexity and mass distribution in gyroids then makes the gyroids printing with BMD more difficult than BMD of other geometries for which the two-beads wall limitation acts. It is the large aspect ratio of the walls together with their small wall footprint, that generates this problem when unsupported gyroid are printed. This problem is exacerbated for gyroids with large Cell Size and low Relative Density whereas smaller gyroids suffers less the deriving wall collapse defect during printing. Consequently, the two set of lines i.e., the odds curves on one side and the iso-thickness on the other, diverge for smaller Cell Size L, whereas the actual printability limit moves toward smaller thicknesses.

The map is valid for 17-4 PH gyroids but, interestingly, these outcomes can be reasonably translated into other types of BMD materials (especially the other steels such as the AISI 316 or the 4140) given the high degree of similarities, both in terms of feedstock composition, granulometry and sintering properties. Conversely, the presented results are valid for gyroids produced in 17-4 PH with the finest nozzle configuration. It must be noted that the extension of the above findings to the case of coarser depositions (i.e., adopting for extruding the gyroids the bigger nozzle available, 0.4 mm in diameter) is not viable, because nozzle diameter and printer resolution turned out to be a key-player in the analysis.

Defects generation mechanisms

As discussed in the result section, the most common observed defect is the collapse of an external portion of the gyroid walls in contact with the printing raft (the steel base upon which the part is built), see pictures in Fig.8g and Fig.8j. This defect is observed to increase with L because bigger L imposes bigger overhang as well as bigger wall aspect-ratio. The critical point is in fact when the wall starts to overhang but is not yet connected with the neighbour wall. This happens at a height coordinate of around L/4, given the selected orientation for the gyroid. Therefore, at this critical height, the compression action of the extrusion head results in a bigger bending moment when L is bigger, thus exacerbating the risk of wall detachment from the base, Fig.14(a)/(b). The portion of the wall does not break but simply detaches from the raft probably because its flexural resistance is bigger than the retaining constraint force given by the wall adhesion on the ceramic interlayer substrate, Fig.

14(c). This interpretation is consistent with the observation that gyroid with bigger RD, i.e., with thicker walls, did not show this defect as the adhesion area that can withstand the bending, increases together with the retaining force.

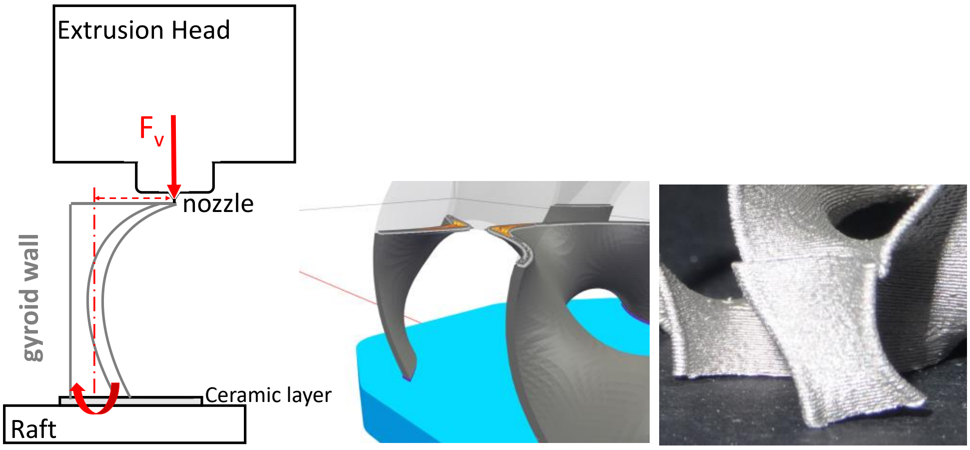

a) b) c)

Fig. 14. Gyroid wall collapse: (a) scheme; (b) slicer toolpath; (c) detachment on the real part

On one side, the knowledge about this defect generation mechanism can possibly enable the development of some design and process optimization that can expand the printability zones but, on the other the complete understanding of the involved phenomena, would need further investigations. In fact, this defect shows random onsets, with respect to the design variables L and RD, since different outcomes are produced among the printing replicas (as depicted in Fig.15, there are situations where some replicas did not show this defect, while other did). Quite interestingly, this failure condition does not show a completely deterministic behavior as observed in Fig.15, where only one gyroid out of three replicas is affected by this issue. This observation suggests that fully deterministic approaches for evaluating the printability of AM structures can be not suitable. Approaches like the adopted logistic regression are inherently capable, indeed, to deal with this uncertainty.

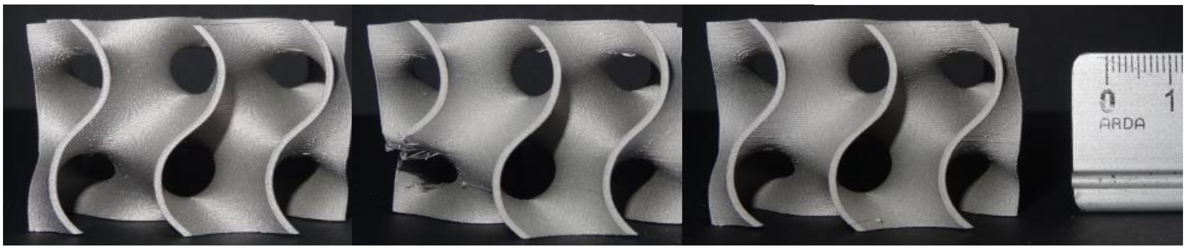

Fig. 15 Sintered gyroids with L=30 mm, RD=0.1 (Replicas 1/2/3)

It must be said that the problem of wall detachment and partial collapse can be mitigated by adopting selective supports (i.e., external local supports applied only in that portion of the gyroid). However, in BMD no local (but only global) external supports can be selected by the users. The impact of this type of defect on single-cell specimen is detrimental but it is for sure less defective on multicellular structures affected by distributed loading conditions. In BMD printing of gyroids however, the use of removable supports [37] is not straightforward since their large presence generate interference with the shrinkage occurrence during furnace treatment, causing cracking, Fig.16

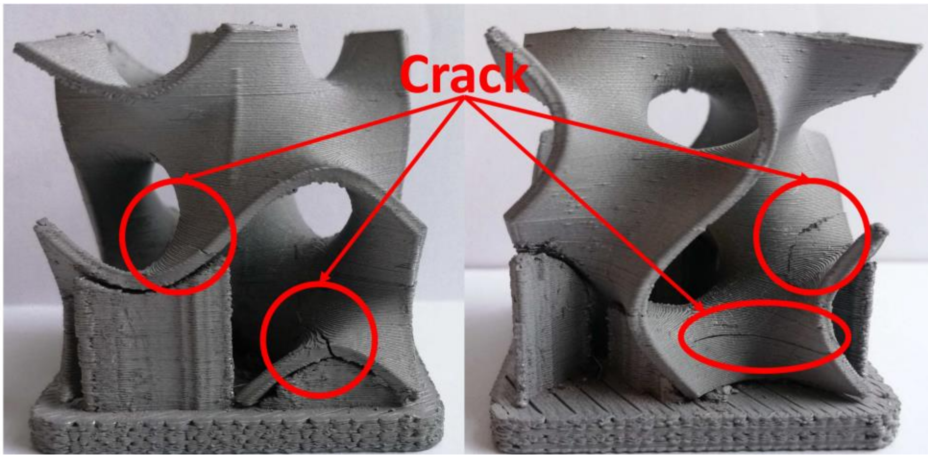

Fig. 16 Pure single-cell sintered gyroid (1L x 1L x 1L, see Fig.5) printed with supports and affected by cracking after sintering (L=40 mm, RD=0.15)

Conclusions

This work provides a method for robust characterization of manufacturability limits of complex TPMS geometries produced by metal FFF approach via Bound Metal Deposition.

The printability analysis is focused on small Schoen-Gyroids (sheet-network type) in 17-4 PH steel being this type most of interest for different TPMS application domains. The case of unsupported single cells gyroids is studied as the most demanding geometrical case. The method provides an estimation of the areas, in the design space of gyroids, where BMD printability is guaranteed from areas where it is denied. This method then enables the integration of the BMD process knowledge into the functional design of any type of complex sheet lattice structures, in a design-for-BMD fashion. By tailoring the quality objective functions on specific needs, the proposed modelling approach can drive designers and technologists through good process setup of support-free steel gyroid cells with different geometrical parameters. It gives a ready, usable tool for designing the gyroids not only basing on the expected functional thermo-mechanical behaviors but also considering their actual manufacturability through BMD.

The innovation of the method comes from the application of a logistic regression model, which is identified starting from a large experimental dataset of gyroid printings. It provides the BMD processing window in metal single-cell unsupported gyroids by quantifying the statistical probability to achieve good printing results with specific combinations of gyroids' geometrical parameters, such as Relative Density and Cell Size. Its strength consists in the capacity to deal with uncertain process performances and in the capacity to integrate acceptance quality criteria that are both qualitative and quantitative. The proposed methodology is powerful since it easily adapts to any type of printed geometries, build materials and quality judgment criteria but also to different manufacturing processes. The identification of this probabilistic model lies on a specific quality assessment of the sintered parts, that leverages on the classification of the observed defects raising during the steps of the BMD process-chain. The adopted binary logistic regression model works successfully with the obtained experimental dataset, providing good fitting conditions and good discriminatory capacity.

In the end, there are some key findings of this work about the BMD printability of steel gyroids, as follows:

- BMD proved to be suitable for unsupported steel gyroid production in a clear portion of design space defined by L and RD in the range of 10-30 mm and 4%-36.8%, respectively.
- The unfeasible BMD printing area of gyroids is larger than the nominal one based on the suggested minimum printable thickness of 0.6 mm. It is therefore not possible to derive the gyroid printability only by relying on the manufacturer prescriptions on the printable minimum wall thickness.
- All the single-cell gyroids with thickness greater than 1 mm can be successfully printed and sintered. Gyroid with smaller thickness can be obtained only when they are small in Cell Size (L< 15 mm). Printability is confirmed for all the tested unit cell gyroids having a Relative Density bigger than 20%.
- The printing success rate curves do not completely match with the iso-thickness lines showing that process BMD sensitivity is larger when the gyroids size is larger than 20 mm, increasing the risk to occur into printing and sintering fails.

Future developments

This initial study on single-cell gyroid represents the baseline for supporting further assessments on the BMD printability of complex multicellular TPMS domains, involving also thermo-mechanical functional characterization.
Starting from the characterised feasibility area of unsupported single-cell gyroids done here, further work can be dedicated to study how the presence of favourable cell boundaries improves the BMD printability, thus extending the printability area toward larger Cell Size. For instance, BMD benefits from the use of bounding box (i.e., flat walls that encloses the gyroid) or the printing of multicellular structures in the X-Y plane (printing one layer of connected cells side-by-side). At the same time, further studies will be dedicated to evaluating the BMD printability of stacked unsupported cells, (i.e., printing a structure with different cells piled up vertically), since the additional effects played by the gravity loads in sintering (due to the self-weight), can play important roles.
The logistic regression methodology will be extended to include the role of the BMD process parameters moving toward the optimization of the printing capability of TPMS based structures. Another worthful point will be analysing different printing materials enabled by BMD production, such as copper, that are receiving strong recent attention from multiple industrial fields regarding the studied geometry.
Finally, cost-assessment and cost-comparison in steel gyroids BMD production is another future aspect to investigate given the opportunities of cost reduction provided by BMD technique with respect to industrial available L-PBF and E-PBF technologies.

Acknowledgments
The present research was partially funded by "Progetto di ricerca S.I.ADD. – Soluzioni Innovative per la qualità e la sostenibilità dei processi di ADDitive manufacturing "MIUR ARS01_00806".
The Italian Ministry of Education, University and Research is acknowledged for the support provided through the Project "Department of Excellence LIS4.0 - Lightweight and Smart Structures for Industry 4.0".

Conflict of interest
None declared.

Declaration of Competing Interest
The authors report no declarations of interest.

Data availability
The raw/processed data required to reproduce these findings cannot be shared at this time as the data also forms part of an ongoing study

References
[1] J. Jiang, Y. Xiong, Z. Zhang, D.W. Rosen, Machine learning integrated design for additive manufacturing, J. Intell. Manuf. (2020). https://doi.org/10.1007/s10845-020-01715-6.
[2] T. Maconachie, M. Leary, B. Lozanovski, X. Zhang, M. Qian, O. Faruque, M. Brandt, SLM lattice structures: Properties, performance, applications and challenges, Mater. Des. 183 (2019) 108137. https://doi.org/10.1016/j.matdes.2019.108137.
[3] J. Brennan-Craddock, D. Brackett, R. Wildman, R. Hague, The design of impact absorbing structures for additive manufacture, J. Phys. Conf. Ser. 382 (2012). https://doi.org/10.1088/1742-6596/382/1/012042.
[4] N.A. Fleck, V.S. Deshpande, M.F. Ashby, Micro-architectured materials: Past, present and future, Proc. R. Soc. A Math. Phys. Eng. Sci. 466 (2010) 2495–2516. https://doi.org/10.1098/rspa.2010.0215.
[5] I. Maskery, L. Sturm, A.O. Aremu, A. Panesar, C.B. Williams, C.J. Tuck, R.D. Wildman, I.A. Ashcroft, R.J.M. Hague, Insights into the mechanical properties of several triply periodic minimal surface lattice structures made by polymer additive manufacturing, Polymer (Guildf). 152 (2018) 62–71. https://doi.org/10.1016/j.polymer.2017.11.049.
[6] O. Al-Ketan, R. Rowshan, R.K. Abu Al-Rub, Topology-mechanical property relationship of 3D printed strut, skeletal, and sheet based periodic metallic cellular materials, Addit. Manuf. 19 (2018) 167–183. https://doi.org/10.1016/j.addma.2017.12.006.
[7] A. Bagheri Saed, A.H. Behravesh, S. Hasannia, S.A. Alavinasab Ardebili, B. Akhoundi, M. Pourghayoumi, Functionalized poly L-lactic acid synthesis and optimization of process parameters for 3D printing of porous scaffolds via digital light processing (DLP) method, J. Manuf. Process. 56 (2020) 550–561. https://doi.org/10.1016/j.jmapro.2020.04.076.
[8] L. Yuan, S. Ding, C. Wen, Additive manufacturing technology for porous metal implant applications and triple minimal surface structures: A review, Bioact. Mater. 4 (2019) 56–70.

https://doi.org/10.1016/j.bioactmat.2018.12.003.

[9] D.W. Abueidda, M. Bakir, R.K. Abu Al-Rub, J.S. Bergström, N.A. Sobh, I. Jasiuk, Mechanical properties of 3D printed polymeric cellular materials with triply periodic minimal surface architectures, Mater. Des. 122 (2017) 255–267. https://doi.org/10.1016/j.matdes.2017.03.018.

[10] C. Yan, L. Hao, A. Hussein, P. Young, D. Raymont, Advanced lightweight 316L stainless steel cellular lattice structures fabricated via selective laser melting, Mater. Des. 55 (2014) 533–541. https://doi.org/10.1016/j.matdes.2013.10.027.

[11] J. Podroužek, M. Marcon, K. Ninčević, R. Wan-Wendner, Bio-inspired 3D infill patterns for additive manufacturing and structural applications, Materials (Basel). 12 (2019) 1–12. https://doi.org/10.3390/ma12030499.

[12] J. Kim, D.J. Yoo, 3D printed compact heat exchangers with mathematically defined core structures, J. Comput. Des. Eng. 7 (2020) 527–550. https://doi.org/10.1093/jcde/qwaa032.

[13] D. Tang, Y. Wang, K. Cheng, Simulation and optimization of lightweight insulating geopolymer composites via dual gradient slurry deposition, J. Manuf. Process. 71 (2021) 249–259. https://doi.org/10.1016/j.jmapro.2021.09.034.

[14] S. Catchpole-Smith, R.R.J. Sélo, A.W. Davis, I.A. Ashcroft, C.J. Tuck, A. Clare, Thermal conductivity of TPMS lattice structures manufactured via laser powder bed fusion, Addit. Manuf. 30 (2019). https://doi.org/10.1016/j.addma.2019.100846.

[15] R.R.J. Sélo, S. Catchpole-Smith, I. Maskery, I. Ashcroft, C. Tuck, On the thermal conductivity of AlSi10Mg and lattice structures made by laser powder bed fusion, Addit. Manuf. 34 (2020) 101214. https://doi.org/10.1016/j.addma.2020.101214.

[16] S. Vijayavenkataraman, L. Zhang, S. Zhang, J.Y.H. Fuh, W.F. Lu, Triply periodic minimal surfaces sheet scaffolds for tissue engineering applications: An optimization approach toward biomimetic scaffold design, ACS Appl. Bio Mater. 1 (2018) 259–269. https://doi.org/10.1021/acsabm.8b00052.

[17] C. Yan, L. Hao, A. Hussein, Q. Wei, Y. Shi, Microstructural and surface modifications and hydroxyapatite coating of Ti-6Al-4V triply periodic minimal surface lattices fabricated by selective laser melting, Mater. Sci. Eng. C. 75 (2017) 1515–1524. https://doi.org/10.1016/j.msec.2017.03.066.

[18] C. Yan, L. Hao, A. Hussein, P. Young, Ti-6Al-4V triply periodic minimal surface structures for bone implants fabricated via selective laser melting, J. Mech. Behav. Biomed. Mater. 51 (2015) 61–73. https://doi.org/10.1016/j.jmbbm.2015.06.024.

[19] C.N. Kelly, C. Kahra, H.J. Maier, K. Gall, Processing, Structure, and Properties of Additively Manufactured Titanium Scaffolds with Gyroid-Sheet Architecture, Addit. Manuf. 41 (2021) 101916. https://doi.org/10.1016/j.addma.2021.101916.

[20] J. Gonzalez-Gutierrez, S. Cano, S. Schuschnigg, C. Kukla, J. Sapkota, C. Holzer, Additive manufacturing of metallic and ceramic components by the material extrusion of highly-filled polymers: A review and future perspectives, Materials (Basel). 11 (2018). https://doi.org/10.3390/ma11050840.

[21] A. Mostafaei, A.M. Elliott, J.E. Barnes, F. Li, W. Tan, C.L. Cramer, P. Nandwana, M. Chmielus, Binder jet 3D printing—Process parameters, materials, properties, modeling, and challenges, Prog. Mater. Sci. 119 (2021) 100707. https://doi.org/10.1016/j.pmatsci.2020.100707.

[22] M. Sadaf, M. Bragaglia, F. Nanni, A simple route for additive manufacturing of 316L stainless steel via Fused Filament Fabrication, J. Manuf. Process. 67 (2021) 141–150. https://doi.org/10.1016/j.jmapro.2021.04.055.

[23] L. Waalkes, J. Längerich, F. Holbe, C. Emmelmann, Feasibility study on piston-based feedstock fabrication with Ti-6Al-4V metal injection molding feedstock, Addit. Manuf. 35 (2020) 101207. https://doi.org/10.1016/j.addma.2020.101207.

[24] P. Singh, V.K. Balla, S. V. Atre, R.M. German, K.H. Kate, Factors affecting properties of Ti-6Al-4V alloy additive manufactured by metal fused filament fabrication, Powder Technol. 386 (2021) 9–19. https://doi.org/10.1016/j.powtec.2021.03.026.

[25] A. Bose, C.A. Schuh, J.C. Tobia, N. Tuncer, N.M. Mykulowycz, A. Preston, A.C. Barbati, B. Kernan, M.A. Gibson, D. Krause, T. Brzezinski, J. Schroers, R. Fulop, J.S. Myerberg, M. Sowerbutts, Y.M. Chiang, A. John Hart, E.M. Sachs, E.E. Lomeli, A.C. Lund, Traditional and additive manufacturing of a new Tungsten heavy alloy alternative, Int. J. Refract. Met. Hard Mater. 73 (2018) 22–28. https://doi.org/10.1016/j.ijrmhm.2018.01.019.

[26] B. Song, C. Kenel, D.C. Dunand, 3D ink-extrusion printing and sintering of Ti, Ti-TiB and Ti-TiC microlattices, Addit. Manuf. 35 (2020) 101412. https://doi.org/10.1016/j.addma.2020.101412.

[27] G. Singh, J.M. Missiaen, D. Bouvard, J.M. Chaix, Copper extrusion 3D printing using metal injection moulding feedstock: Analysis of process parameters for green density and surface roughness optimization, Addit. Manuf. 38 (2021) 101778. https://doi.org/10.1016/j.addma.2020.101778.

[28] N. Dehdari Ebrahimi, Y.S. Ju, Thermal conductivity of sintered copper samples prepared using 3D

printing-compatible polymer composite filaments, Addit. Manuf. 24 (2018) 479–485. https://doi.org/10.1016/j.addma.2018.10.025.

[29] H. Tiismus, A. Kallaste, T. Vaimann, A. Rassolkin, A. Belahcen, Technologies for Additive Manufacturing of Electrical Machines, Int. Conf. Young Spec. Micro/Nanotechnologies Electron Devices, EDM. 2019-June (2019) 651–655. https://doi.org/10.1109/EDM.2019.8823462.

[30] S. Restrepo, S. Ocampo, J.A. Ramirez, C. Paucar, C. Garcia, Mechanical properties of ceramic structures based on Triply Periodic Minimal Surface (TPMS) processed by 3D printing, J. Phys. Conf. Ser. 935 (2017). https://doi.org/10.1088/1742-6596/935/1/012036.

[31] L. Zhang, S. Feih, S. Daynes, S. Chang, M.Y. Wang, J. Wei, W.F. Lu, Pseudo-ductile fracture of 3D printed alumina triply periodic minimal surface structures, J. Eur. Ceram. Soc. 40 (2020) 408–416. https://doi.org/10.1016/j.jeurceramsoc.2019.09.048.

[32] S. Vijayavenkataraman, L.Y. Kuan, W.F. Lu, 3D-printed ceramic triply periodic minimal surface structures for design of functionally graded bone implants, Mater. Des. 191 (2020) 108602. https://doi.org/10.1016/j.matdes.2020.108602.

[33] Y. Thompson, J. Gonzalez-Gutierrez, C. Kukla, P. Felfer, Fused filament fabrication, debinding and sintering as a low cost additive manufacturing method of 316L stainless steel, Addit. Manuf. 30 (2019) 100861. https://doi.org/10.1016/j.addma.2019.100861.

[34] A.I. Nurhudan, S. Supriadi, Y. Whulanza, A.S. Saragih, Additive manufacturing of metallic based on extrusion process: A review, J. Manuf. Process. 66 (2021) 228–237. https://doi.org/10.1016/j.jmapro.2021.04.018.

[35] D.W. Abueidda, M. Elhebeary, C.S. (Andrew) Shiang, S. Pang, R.K. Abu Al-Rub, I.M. Jasiuk, Mechanical properties of 3D printed polymeric Gyroid cellular structures: Experimental and finite element study, Mater. Des. 165 (2019) 107597. https://doi.org/10.1016/j.matdes.2019.107597.

[36] T. Maconachie, R. Tino, B. Lozanovski, M. Watson, A. Jones, C. Pandelidi, A. Alghamdi, A. Almalki, D. Downing, M. Brandt, M. Leary, The compressive behaviour of ABS gyroid lattice structures manufactured by fused deposition modelling, Int. J. Adv. Manuf. Technol. 107 (2020) 4449–4467. https://doi.org/10.1007/s00170-020-05239-4.

[37] Desktop Metal - accessed on 1st may 2021, https://www.desktopmetal.com/, (n.d.).

[38] J. Jiang, X. Xu, J. Stringer, Support Structures for Additive Manufacturing: A Review, J. Manuf. Mater. Process. 2 (2018). https://doi.org/10.3390/jmmp2040064.

[39] S. Singh, G. Singh, C. Prakash, S. Ramakrishna, Current status and future directions of fused fi lament fabrication, J. Manuf. Process. 55 (2020) 288–306. https://doi.org/10.1016/j.jmapro.2020.04.049.

[40] A. Watson, J. Belding, B.D. Ellis, Characterization of 17-4 PH Processed via Bound Metal Deposition (BMD), Miner. Met. Mater. Ser. (2020) 205–216. https://doi.org/10.1007/978-3-030-36296-6_19.

[41] F. Tamburrino, S. Graziosi, M. Bordegoni, The design process of additively manufactured mesoscale lattice structures: A review, J. Comput. Inf. Sci. Eng. 18 (2018) 1–16. https://doi.org/10.1115/1.4040131.

[42] W. Elmadih, W.P. Syam, I. Maskery, D. Chronopoulos, R. Leach, Mechanical vibration bandgaps in surface-based lattices, Addit. Manuf. 25 (2019) 421–429. https://doi.org/10.1016/j.addma.2018.11.011.

[43] D. Barba, E. Alabort, R.C. Reed, Synthetic bone: Design by additive manufacturing, Acta Biomater. 97 (2019) 637–656. https://doi.org/10.1016/j.actbio.2019.07.049.

[44] I. Echeta, X. Feng, B. Dutton, R. Leach, S. Piano, Review of defects in lattice structures manufactured by powder bed fusion, Int. J. Adv. Manuf. Technol. 106 (2020) 2649–2668. https://doi.org/10.1007/s00170-019-04753-4.

[45] O. Al-Ketan, M. Ali, M. Khalil, R. Rowshan, K.A. Khan, R.K. Abu Al-Rub, Forced Convection Computational Fluid Dynamics Analysis of Architected and Three-Dimensional Printable Heat Sinks Based on Triply Periodic Minimal Surfaces, J. Therm. Sci. Eng. Appl. 13 (2021) 1–14. https://doi.org/10.1115/1.4047385.

[46] D. Mahmoud, K.S. Al-Rubaie, M.A. Elbestawi, The influence of selective laser melting defects on the fatigue properties of Ti6Al4V porosity graded gyroids for bone implants, Int. J. Mech. Sci. 193 (2021). https://doi.org/10.1016/j.ijmecsci.2020.106180.

[47] L. Zhang, S. Feih, S. Daynes, S. Chang, M.Y. Wang, J. Wei, W.F. Lu, Energy absorption characteristics of metallic triply periodic minimal surface sheet structures under compressive loading, Addit. Manuf. 23 (2018) 505–515. https://doi.org/10.1016/j.addma.2018.08.007.

[48] Y. Jin, H. Kong, X. Zhou, G. Li, J. Du, Design and characterization of sheet-based gyroid porous structures with bioinspired functional gradients, Materials (Basel). 13 (2020). https://doi.org/10.3390/ma13173844.

[49] I. Maskery, N.T. Aboulkhair, A.O. Aremu, C.J. Tuck, I.A. Ashcroft, Compressive failure modes and

energy absorption in additively manufactured double gyroid lattices, Addit. Manuf. 16 (2017) 24–29. https://doi.org/10.1016/j.addma.2017.04.003.
[50] H. Yin, Z. Liu, J. Dai, G. Wen, C. Zhang, Crushing behavior and optimization of sheet-based 3D periodic cellular structures, Compos. Part B Eng. 182 (2020) 107565. https://doi.org/10.1016/j.compositesb.2019.107565.
[51] S. Liu, A.P. Stebner, B.B. Kappes, X. Zhang, Machine learning for knowledge transfer across multiple metals additive manufacturing printers, Addit. Manuf. 39 (2021) 101877. https://doi.org/10.1016/j.addma.2021.101877.
[52] A.P. Garland, B.C. White, B.H. Jared, M. Heiden, E. Donahue, B.L. Boyce, Deep Convolutional Neural Networks as a Rapid Screening Tool for Complex Additively Manufactured Structures, Addit. Manuf. 35 (2020). https://doi.org/10.1016/j.addma.2020.101217.
[53] M. Strano, B.M. Colosimo, Logistic regression analysis for experimental determination of forming limit diagrams, Int. J. Mach. Tools Manuf. 46 (2006) 673–682. https://doi.org/10.1016/j.ijmachtools.2005.07.005.
[54] O. Al-Ketan, R.K. Abu Al-Rub, MSLattice: A free software for generating uniform and graded lattices based on triply periodic minimal surfaces, Mater. Des. Process. Commun. (2020) 1–10. https://doi.org/10.1002/mdp2.205.
[55] J.C. Tobia, Geometry for debinding 3D printed parts, United States Patent Application, Pub . No . : US 2019 / 0240734 A1, n.d.
[56] T. Hastie, R. Tibshirani, J. Friedman, The Elements of Statistical Learning, (n.d.).
[57] A. Agresti, An Introduction to Categorical Data Analysis Second Edition, n.d.

Appendix A: Regression fitting on the nominal minimum gyroid wall thickness

Table A1: Experimental design and logistic regression Class for the three replicas for a total of 48 gyroids

#Run	**L [mm] Cell Size (Nominal)**	**RD Relative Density (Nominal)**	**t [mm] nominal thickness**	**Replica 1**		**Replica 2**		**Replica 3**	
				Class	Fault	Class	Fault	Class	Fault
1	30	0.040	0.502	1	Collapse	1	Collapse	1	Collapse
2	23	0.045	0.436	1	Collapse	1	Partial collapse/ not detachable from raft	1	Collapse
3	17	0.061	0.445	1	Partial Collapse	1	Partial collapse	1	Partial collapse
4	10	0.082	0.358	1	Agglomerate of Build Media/Printing defects	1	Poor surface quality/printing defects	1	Poor surface quality/printing defects
5	30	0.061	0.783	1	Collapse	1	Collapse	1	Partial collapse
6	23	0.074	0.736	1	Partial Collapse	0	-	0	-
7	17	0.100	0.747	1	Overhang defect	1	Partial collapse/not detachable from raft	0	-
8	10	0.135	0.604	0	-	1	Partial collapse	1	Defective part
9	30	0.100	1.312	0	Slight warpage	1	Partial collapse	0	Slight warpage
10	23	0.122	1.245	0	-	0	Slight warpage	0	-
11	17	0.165	1.265	0	-	0	-	1	-
12	10	0.223	1.023	0	-	0	-	0	-
13	30	0.165	2.227	0	Slight warpage / Build Media Stringing	0	Slight warpage	0	Slight warpage
14	23	0.202	2.114	0	-	0	-	0	-
15	17	0.273	2.147	0	-	0	-	0	-
16	10	0.368	1.733	0	-	0	-	0	-

a)

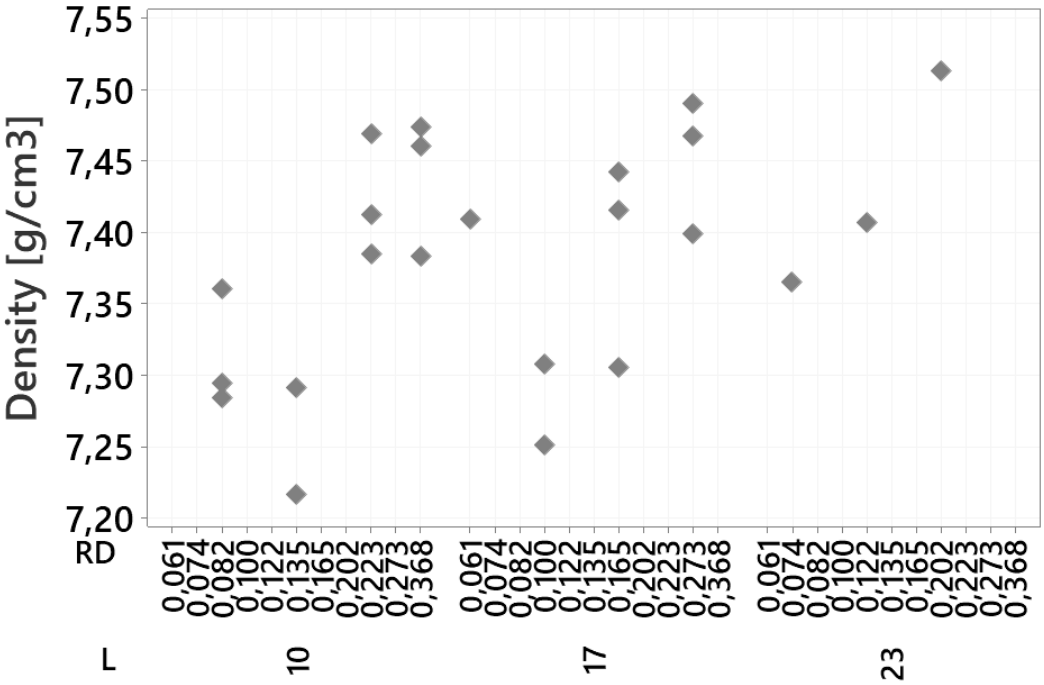

b)

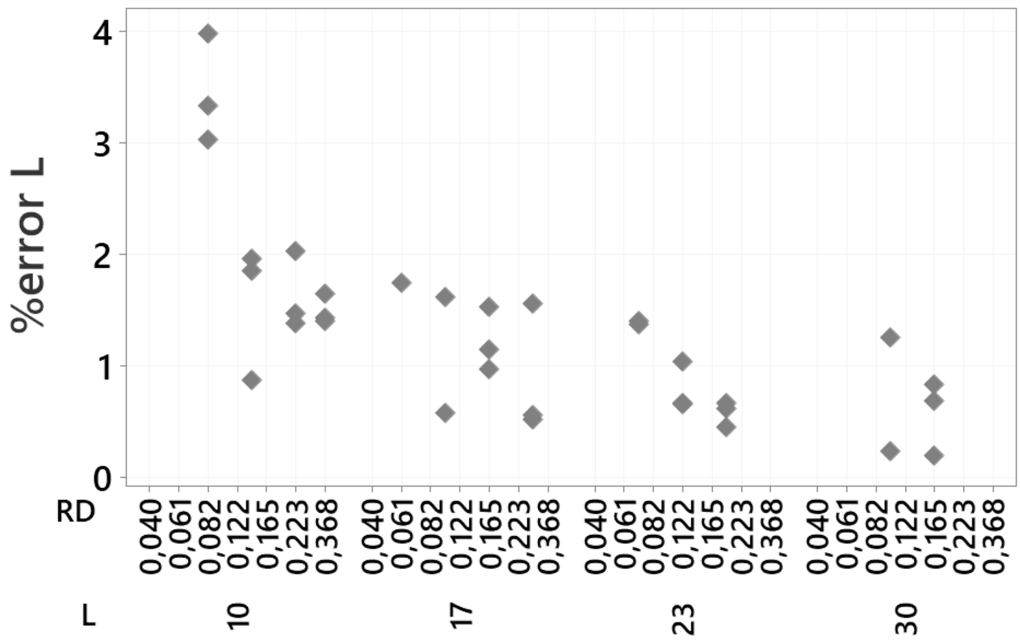

Fig. A1. a) Sintered gyroid material density ρ (nominal density = 7.6 g/cm^3). b) Percentage Errors on actual Cell Size L ((%error L= L_{real} - L / L *100)), average value among the three dimensions). Collapsed parts are not analysed, therefore the related points are missing in the graphs.